

Nonlinear Mach-Zehnder Interferometer as a DPSK Signal Regenerator

Chad Ropp
Dr. Julius Goldhar

Abstract:

Nonlinear Mach-Zehnder interferometers (MZI), when driven by a phase-locked local oscillator pump, provide phase-sensitive amplification to input signals. Phase noise clean up is achieved as a result. Designing the device to operate in saturation with distortion provides added amplitude noise reduction. Using this approach, a scheme for differential phase-shift keyed (DPSK) regeneration is proposed. A steady state model is developed using different nonlinear media including Kerr media, saturable gain, saturable absorption, and two-photon absorption. Comparative analysis of these devices is given with an emphasis on both phase and amplitude regeneration and signal quality as seen by the receiver.

1. Introduction

There are several modulation techniques in consideration for today's optical communication networks aside from classical on/off keying (OOK). One alternative modulation scheme of interest is differential phase-shift keying (DPSK) which assigns bit values to changes in signal phase. In many regards this approach is more robust than OOK. For use in modern communication systems, long distance propagation of signals is necessary. This results in degradation of signal to noise ratio due to signal attenuation and the addition of noise from optical amplifiers. Regenerative devices must be considered to ensure that the signal is recoverable by the receiver and that data is not lost in noise. Compared to OOK signals, which are only affected by amplitude noise, DPSK signals degrade from both phase and amplitude noise. Several past designs for a DPSK regenerator have been proposed using different interferometers including Sagnac ^{[1] [2] [3] [4]} and Mach-Zehnder ^[5]. Sagnac interferometry provides less than substantial regenerative results and this paper will focus primarily on the Mach-Zehnder design proposed by K. Croussore et al. Several nonlinear media will be analyzed and compared for use in this DPSK regeneration scheme.

2. Mathematical Methods

2.1 Methods

All models and simulations are realized using Matlab. In subsequent calculations a time independent model is used. Signal information is stored in phasor notation where each phasor describes the phase and amplitude components of electric fields. Traveling pulses of light are represented discretely as arrays of phasors. In simulating the Mach-Zehnder interferometer, we assume that all components are linear and lossless and that both arms are perfectly symmetric.

For simplification of calculations we will be using unconventional normalized units of electric field (E), intensity (I) and power (P) such that we can disregard geometry and features of the propagating media. Therefore all constant coefficients are dropped and all characteristics of the fiber medium remain unchanged with space and time.

Our units are defined such that:

$$I = P \tag{1}$$

$$|\vec{E}| = \sqrt{I} \tag{2}$$

2.2 The Optical Beam Splitter

The optical beam splitter is the primary optical device used in a Mach-Zehnder interferometer (MZI). The optical beam splitter is an optical interface where an incident wave is partially reflected and partially transmitted. We will be dealing with 50:50 optical beam splitters where half of the power of the wave is reflected and half is transmitted. The phasors ρ and τ are complex vectors that describe both the magnitude and phase change for both reflected and transmitted electrical field waves, respectively as seen below in Figure 1.

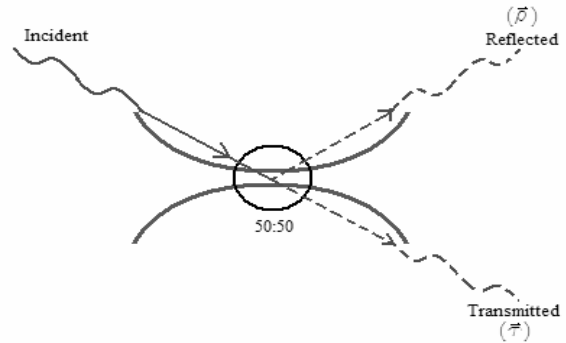


Figure 1: One Input Optical Beam Splitter

By conservation of energy it can be shown that:

$$\rho^* \tau + \rho \tau^* = 0 \tag{3}$$

$$|\rho|^2 + |\tau|^2 = 1 \tag{4}$$

From Equations 3 and 4 ρ and τ are found to be 90° out of phase from one another. Also since we are dealing with a 50:50 beam splitter, their magnitudes squared are equal to one half. Without loss of generality we can assign τ to be entirely real and ρ to be entirely imaginary. The assignments in Equation 5 satisfy both Equations 3 and 4.

$$\begin{aligned} \tau &= \sqrt{\frac{1}{2}} \\ \rho &= j\sqrt{\frac{1}{2}} \end{aligned} \tag{5}$$

The electric fields of the reflected and transmitted waves are found to be:

$$\hat{E}_{trans} = \sqrt{\frac{1}{2}}\hat{E}_{inc} \quad (6)$$

$$\hat{E}_{refl} = j\sqrt{\frac{1}{2}}\hat{E}_{inc} \quad (7)$$

With two incident waves of the same frequency, phasor representation of electric fields and the rule of superposition can be used to describe the waves as they travel through the optical beam splitter, see Figure 2.

$$\begin{aligned} \hat{E}_{out_1} &= \hat{E}_{refl_1} + \hat{E}_{trans_2} \\ &= j\sqrt{\frac{1}{2}}\hat{E}_{inc_1} + \sqrt{\frac{1}{2}}\hat{E}_{inc_2} \end{aligned} \quad (8a)$$

$$\begin{aligned} \hat{E}_{out_2} &= \hat{E}_{trans_1} + \hat{E}_{refl_2} \\ &= \sqrt{\frac{1}{2}}\hat{E}_{inc_1} + j\sqrt{\frac{1}{2}}\hat{E}_{inc_2} \end{aligned} \quad (8b)$$

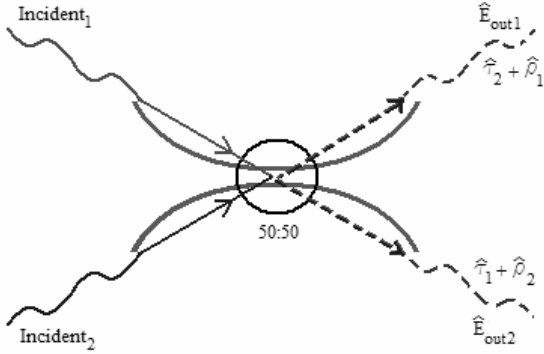


Figure 2: Two Input Optical Beam Splitter

2.3 The Linear MZI

The linear MZI, shown in Figure 3, is simply two optical beam splitters in series such that the output of the first becomes the input of the second.

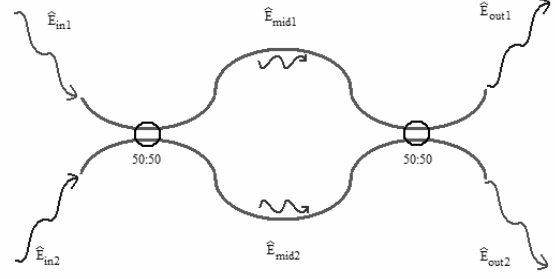


Figure 3: Linear Mach-Zehnder Interferometer

Equations 9a and 9b show that the magnitude of the outputs of the linear MZI equal the magnitude of the inputs. Phase differences at the input are also preserved at the output. These characteristics are only true for the linear MZI.

$$\begin{aligned} \hat{E}_{out_1} &= j\sqrt{\frac{1}{2}}\hat{E}_{mid_1} + \sqrt{\frac{1}{2}}\hat{E}_{mid_2} \\ &= j\sqrt{\frac{1}{2}}\left(j\sqrt{\frac{1}{2}}\hat{E}_{inc_1} + \sqrt{\frac{1}{2}}\hat{E}_{inc_2}\right) + \sqrt{\frac{1}{2}}\left(\sqrt{\frac{1}{2}}\hat{E}_{inc_1} + j\sqrt{\frac{1}{2}}\hat{E}_{inc_2}\right) \\ &= -\frac{1}{2}\hat{E}_{inc_1} + j\frac{1}{2}\hat{E}_{inc_2} + \frac{1}{2}\hat{E}_{inc_1} + j\frac{1}{2}\hat{E}_{inc_2} \\ &= j\hat{E}_{inc_2} \end{aligned} \quad (9a)$$

$$\begin{aligned} \hat{E}_{out_2} &= \sqrt{\frac{1}{2}}\hat{E}_{mid_1} + j\sqrt{\frac{1}{2}}\hat{E}_{mid_2} \\ &= \sqrt{\frac{1}{2}}\left(j\sqrt{\frac{1}{2}}\hat{E}_{inc_1} + \sqrt{\frac{1}{2}}\hat{E}_{inc_2}\right) + j\sqrt{\frac{1}{2}}\left(\sqrt{\frac{1}{2}}\hat{E}_{inc_1} + j\sqrt{\frac{1}{2}}\hat{E}_{inc_2}\right) \\ &= j\frac{1}{2}\hat{E}_{inc_1} + \frac{1}{2}\hat{E}_{inc_2} + j\frac{1}{2}\hat{E}_{inc_1} - j\frac{1}{2}\hat{E}_{inc_2} \\ &= j\hat{E}_{inc_1} \end{aligned} \quad (9b)$$

2.4 Kerr Media

2.4i Kerr Effect

Kerr media have the property that their refractive index depends on the intensity of the wave passing through it.

The relationship is described by ^[6]:

$$n = n_0 + n_2 I \quad (10)$$

The Kerr Effect is determined by a material's third order electric susceptibility, $\chi^{(3)}$, which is proportional to n_2 . The change in phase associated with a material interface is a result of the change in refrac-

tive index. We are interested in the nonlinear index, n_2 , which provides Kerr media with the ability to self-phase modulate. The Kerr media of choice for many applications is highly nonlinear fiber (HNLF), which we will be using for calculations.

2.4ii Nonlinear MZI with Kerr Media

When two HNLFs of equal electric susceptibility and length are introduced into the arms of a linear MZI the device becomes unbalanced such that Equations 9a and 9b are no longer true.

To distinguish our inputs we name one the local oscillator (LO) pump and the other the signal. The output of interest is diagonal from the signal input. If we were dealing with a linear MZI like in equation 9a, this output would correspond to the one that yielded the signal input back out. Figure 4 demonstrates this labeling scheme. For simplicity of calculations the LO will have a phase of zero, making its phasor representation entirely real. The signal's phasor notation will include phase and it will define the relative phase difference between it and the LO.

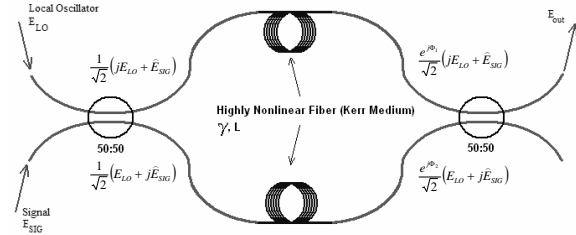


Figure 4: Nonlinear MZI with HNLF

The nonlinear phase shifts in each HNLF are labeled Φ_1 and Φ_2 for the top and bottom arms of the MZI respectively.

The phase shift for Kerr media is given by [6]:

$$\Phi = \frac{2\pi}{\lambda} n_2 L I \quad (11)$$

or

$$\Phi = \frac{2\pi}{\lambda} n_2 L (\hat{E}\hat{E}^*) \quad (12)$$

A common constant used to describe the characteristics of a Kerr medium is γ in units of $W^{-1} km^{-1}$ which is defined as the following:

$$\gamma = \frac{2\pi n_2}{\lambda} \quad (13)$$

Using Equations 12 and 13 the nonlinear phase shift through both arms of the MZI are calculated:

$$\Phi_1 = \gamma L \left(\frac{(jE_{LO} + \hat{E}_{SIG})}{\sqrt{2}} \frac{(-jE_{LO} + \hat{E}_{SIG}^*)}{\sqrt{2}} \right) \quad (14a)$$

$$\Phi_2 = \gamma L \left(\frac{(E_{LO} + j\hat{E}_{SIG})}{\sqrt{2}} \frac{(E_{LO} - j\hat{E}_{SIG}^*)}{\sqrt{2}} \right) \quad (14b)$$

The output of this nonlinear MZI can be written as:

$$\hat{E}_{out} = \frac{E_{LO}}{2} (e^{j\Phi_2} - e^{j\Phi_1}) + j \frac{\hat{E}_{SIG}}{2} (e^{j\Phi_2} + e^{j\Phi_1}) \quad (15)$$

Equation 15 shows that the output is comprised of a mix of signal and LO. The proportion of the mix is described by the differences in the exponential terms with the nonlinear phase shifts. If the difference in phase shift across the arms of the MZI is large, more of the LO and less of the signal makes it to the output. Equations 14a and 14b show that these phase shifts are related to the input electric fields, specifically the phase difference between them. Since excess power from the pump can be diverted to the output and controlled by the input phase of the signal, a phase-sensitive amplifier can be created. As will be shown later this can be done with other nonlinear media other than just Kerr media.

To demonstrate this, if we have a 10mW LO and a 1mW signal passing through an ideal nonlinear MZI with 10km of HNLF with a characteristic $\gamma = 10 W^{-1} km^{-1}$ we see phase-sensitive amplification, shown below.

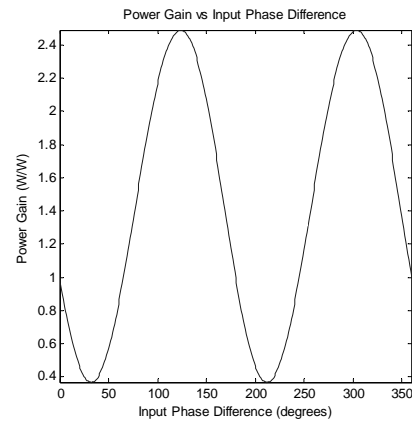


Figure 5: HNLF Phase-Sensitive Amplifier

2.5 Saturable Amplifiers

2.5i Gain Characteristics

Saturable amplifiers are another type of nonlinear media. We will be specifically looking at the characteristics of semiconductor optical amplifiers (SOAs). The SOA is an electrically powered waveguide that acts to amplify optical signals passing through it. There is an effective exponential power gain of the device, g_0 which commercially has a range of about 2 to 6 nepers per unit length. Saturable devices are described by their saturation power, P_{SAT} . We will be using a P_{SAT} of 1mW for all subsequent calculations.

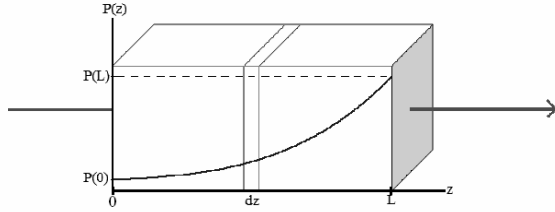


Figure 6: Saturable Amplifier

In SOAs power in the z-direction, shown above, satisfies the following differential equation [7] [8]:

$$\frac{1}{P(z)} \frac{dP(z)}{dz} = \frac{g_0}{1 + \frac{P(z)}{P_{SAT}}} \quad (16)$$

The solution to Equation 16 can be written in implicit algebraic form as:

$$\ln\left(\frac{P(L)}{P(0)}\right) + \left(\frac{P(L) - P(0)}{P_{SAT}}\right) = g_0 L \quad (17)$$

Matlab can be used to solve Equation 17 and provide a more compact form for $P(L)$. This form, shown below, can be used in Matlab simulations so that Equation 17 does not have to be solved numerically every time.

$$P(L) = P_{SAT} \cdot \text{LAMBERTW}\left(\frac{P(0)}{P_{SAT}} e^{\frac{P(0)}{P_{SAT}} + g_0 L}\right) \quad (18)$$

The LAMBERTW function is defined as the solution to:

$$\text{LAMBERTW}(X): X = We^w \quad (19)$$

The gain of the device is defined as:

$$G = \frac{P(L)}{P(0)} = \frac{I_{OUT}}{I_{IN}} \quad (20)$$

The exponential gain is:

$$g = \ln(G) \quad (21)$$

2.5ii Phase Characteristics

The SOA also varies the affects the phase of the electric field as it propagates through it. This change in phase depends on the Henry-alpha factor, α_H , of the media which is the ratio between the real and imaginary parts of gain. Typical values for the Henry-alpha factor are 3-5.

After solving Equation 17 and calculating the exponential gain of the device, the output electric field component with its phase change is found to be:

$$\hat{E}(L) = \hat{E}(0) e^{\frac{g}{2}(1 + j\alpha_H)} \quad (22)$$

$$\hat{E}(L) = \sqrt{I(L)} e^{j\left(\frac{g}{2}\alpha_H + \theta_n\right)} \quad (23)$$

The output phase is easily seen below from Equation 23.

$$\theta_{out} = \frac{g}{2}\alpha_H + \theta_{in} \quad (24)$$

A model of the SOA can be seen in Figure 7.



Figure 7: Semiconductor Optical Amplifier

2.5iii Amplified Spontaneous Emission

One drawback to using optical amplifiers is that noise that is spontaneously emitted along the length of the media also gets amplified.

Using the model of one photon emission per mode per bandwidth and the notion that the SOA is operating with only one mode the equation for amplified spontaneous emission (ASE) is [9] [10].

$$I_{ASE} = \hbar\omega \cdot (\Delta\nu) \cdot (G - 1) \quad (25)$$

Substituting typical optical values for bandwidth, 100GHz, and wavelength, 1.5 μ m:

$$I_{ASE} = 1.325 \times 10^{-8} \cdot (G-1) \quad (26)$$

Since we are dealing with electric field phasors in our calculations, note that the direction in which this noise is arranged is completely random.

$$\hat{E}_{ASE} = \sqrt{1.325 \times 10^{-8} \cdot (G-1)} \cdot e^{j\theta_{random}} \quad (27)$$

The overall output of the SOA is the sum of what was calculated in Equations 21 and 27. It is important to note that when the input signal intensity is much larger than one photon per mode per bandwidth the ASE noise gets overshadowed by the signals themselves and their effect is reduced.



Figure 8: SOA with Amplified Spontaneous Emission

A more complete model of the SOA is shown above. ASE will play a role in later simulation, however many calculations including optimizations will disregard ASE because we are dealing with simple analytical models that do not characterize noise.

2.5iv Nonlinear MZI with SOA

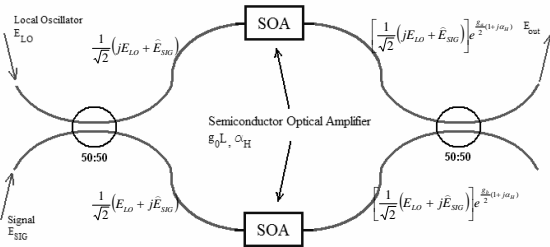


Figure 9: Nonlinear MZI with SOA

The output of a nonlinear MZI with SOA, see above, can be put in the form of Equation 15, the same form as was used to describe the output of the HNLFF-based nonlinear MZI. The difference comes from the definition of Φ_1 and Φ_2 , which are as follows.

$$\Phi_1 = \frac{g_a}{2} (\alpha_H - j) \quad (28a)$$

$$\Phi_2 = \frac{g_b}{2} (\alpha_H - j) \quad (28b)$$

From these equations, the main distinction between SOA and Kerr media can be understood.

Whereas Kerr media had entirely real Φ s, characterizing only nonlinear phase shift, the SOA has complex Φ s which describe both nonlinear amplitude gain and nonlinear phase shift. Despite these differences the SOA-based nonlinear MZI also functions as a phase-sensitive amplifier. Figure 10 was simulated using an I_{SAT} of 1mW, a 100 μ W LO and a 1 μ W signal which were passed through an ideal nonlinear MZI with identical SOAs of $\alpha_H=3$ and $g_0L=3$.

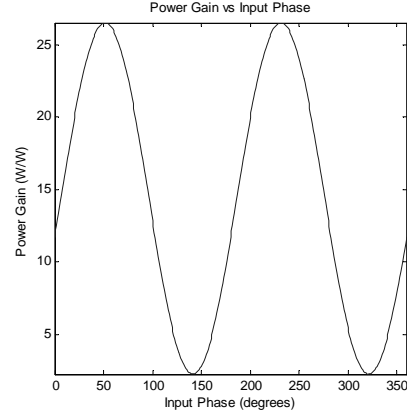


Figure 10: SOA Phase Sensitive Amplifier

2.6 Saturable Absorbers

2.6i Loss Characteristics

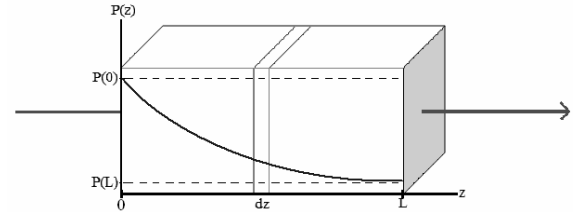


Figure 11: Saturable Absorber

Saturable absorbers (SA) are exactly the same as saturable amplifiers, except instead of providing gain they provide attenuation. As a result the SA does not require input electric power nor is it affected by ASE. In SAs, power in the z-direction, see Figure 11, obeys the same differential equation as power in SOAs^[11].

$$\frac{1}{P(z)} \frac{dP(z)}{dz} = \frac{-\alpha_0}{1 + \frac{P(z)}{P_{SAT}}} \quad (29)$$

The α_0 describes the attenuation, or negative gain, of the device. The same logic that was used for the SOA is used for the SA in calculating P(L).

$$\ln\left(\frac{P(L)}{P(0)}\right) + \left(\frac{P(L) - P(0)}{P_{SAT}}\right) = -\alpha_0 L \quad (30)$$

$$P(L) = P_{SAT} \text{LAMBERTW} \left(\frac{P(0)}{P_{SAT}} e^{\frac{P(0)}{P_{SAT}} \alpha_0 L} \right) \quad (31)$$

The exponential attenuation of the device is defined as:

$$-\alpha = \ln \left(\frac{P(L)}{P(0)} \right) = \ln \left(\frac{I_{OUT}}{I_{IN}} \right) \quad (32)$$

2.6ii Phase Characteristics

The SA also has a Henry-alpha factor to describe the ratio between real and imaginary parts of gain and it follows the same rules as in the SOA.

The output electric field component with its nonlinear change in phase is found to be:

$$\hat{E}(L) = \hat{E}(0) e^{\frac{-\alpha}{2}(1+j\alpha_H)} \quad (33)$$

$$\hat{E}(L) = \sqrt{I(L)} e^{j \left(\frac{-\alpha}{2} \alpha_H + \theta_m \right)} \quad (34)$$

The output phase is seen from Equation 34.

$$\theta_{out} = \frac{-\alpha}{2} \alpha_H + \theta_{in} \quad (35)$$



Figure 12: Saturated Absorber

A complete model of the SA is shown in Figure 12.

2.6iii Nonlinear MZI with SA

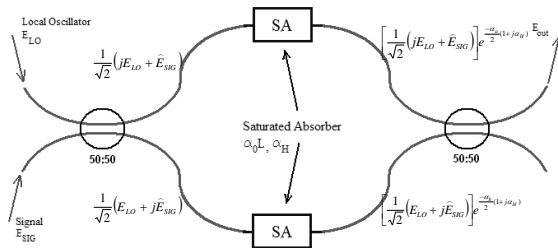


Figure 13: Nonlinear MZI with SA

The output of the nonlinear MZI with SA, see above, is consistent with the form described in Equation 15. Its Φ_1 and Φ_2 are:

$$\Phi_2 = \frac{-\alpha_b}{2} (\alpha_H - j) \quad (36b)$$

$$\Phi_1 = \frac{-\alpha_a}{2} (\alpha_H - j) \quad (36a)$$

This device also functions as a phase-sensitive attenuator, however it is important for it to be operating in or near saturation in order for the contrast between max and min attenuation to be significant. Results are shown in Figure 14 using simulation with an I_{SAT} of 1mW, a 1mW LO and a 100μW signal passing through an ideal nonlinear MZI with identical SAs of $\alpha_H=3$ and $\alpha_0 L=3$.

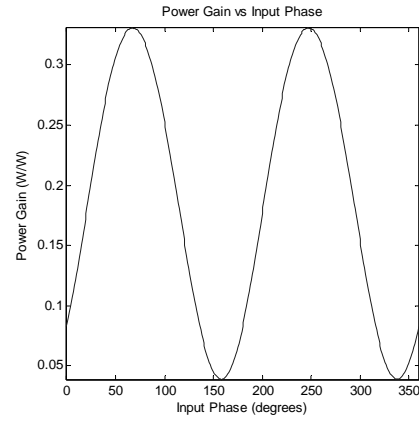


Figure 14: SA Phase-sensitive Amplifier

Although the graph above does not show it, the nonlinear MZI with SA can achieve amplification greater than one. This is allowable for similar reasons as to why the HNL model could achieve amplification even without gain through the nonlinear media. With a large enough pump, loss through the individual SAs can be compensated for by the amplification of the nonlinear SA MZI as a whole and net gain can be achieved.

2.7 Two-Photon Absorbers

2.7i Loss Characteristics

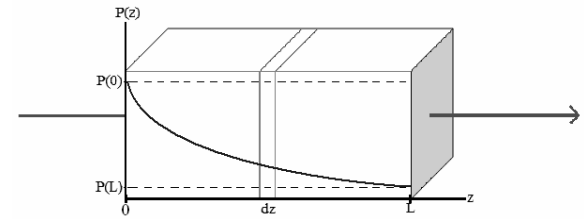


Figure 15: Two-Photon Absorber

The fourth and final nonlinear media of interest considered in this paper is two-photon absorbing (TPA) media, shown above. This media is similar to the SA in that it acts as an intensity dependant absorber, however no nonlinear phase change is experienced and z-directional power in the TPA obeys an entirely different differential equation than in the SA [12].

$$\frac{dP}{dz} = -\alpha_2 P^2 \quad (37)$$

Where α_2 is the attenuation constant of the media

A solution to Equation 37 is found and shown in explicit algebraic form:

$$P(L) = \frac{P(0)}{P(0)\alpha_2 L + 1} \quad (38)$$

Since we assume that TPA material does not have a nonlinear effect on phase change, our model will define the output phase of the TPA to be the same as the input phase.



Figure 16: Two-Photon Absorption

The exponential attenuation of the device is defined as:

$$-\alpha = \ln\left(\frac{P(L)}{P(0)}\right) = \ln\left(\frac{I_{OUT}}{I_{IN}}\right) = \ln\left(\frac{1}{I(0)\alpha_2 L + 1}\right) \quad (39)$$

An equation for the electric field at the output of the TPA media is found to be:

$$\hat{E}(L) = \hat{E}(0)e^{-\frac{\alpha}{2}} \quad (40)$$

$$\hat{E}(L) = \sqrt{I(0)}e^{j\theta_{in} - \frac{\alpha}{2}} \quad (41)$$

2.7ii Nonlinear MZI with TPA

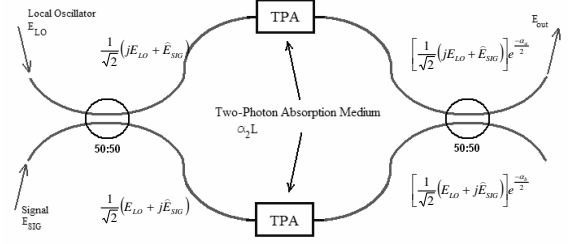


Figure 17: Nonlinear MZI with TPA

The output of the nonlinear MZI with TPA, see above, is also consistent with the form described in Equation 15. Its Φ_1 and Φ_2 are:

$$\Phi_1 = j \frac{\alpha_a}{2} \quad (42a)$$

$$\Phi_2 = j \frac{\alpha_b}{2} \quad (42b)$$

Since there is no nonlinear change in phase through the TPA device it will be interesting to see how it compares to the others when looked at as a phase-sensitive attenuator. The parameters used to simulate were $I_{LO} = 1\text{mW}$, $I_{SIG} = 1\mu\text{W}$, and $\alpha_2 L = 3$ and results are shown below.

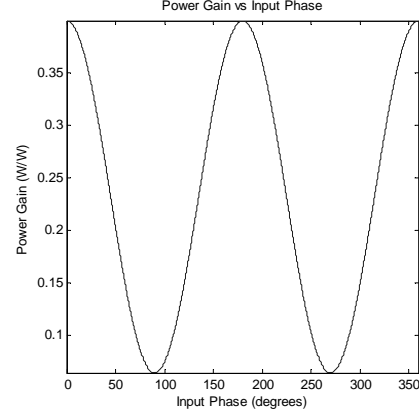


Figure 18: TPA Phase-sensitive Amplifier

The TPA-based nonlinear MZI also has phase-sensitive attenuator qualities, however its graph is symmetric and experiences the least attenuation with an input phase of 0° or 180° and max attenuation at 90° and 270° . Also interesting is the fact that this device cannot provide net amplification of an input signal.

2.8 Differential Phase Shift Keying

Optical DPSK is a method of modulating a signal where a digital “1” corresponds to a 180° phase change and a digital “0” corresponds to a 0° phase change between consecutive propagating bits. Bit comparison at the receiver is necessary because as a signal propagates its phase changes, however relative phase differences between bits do not. This is true because normal fibers used for the propagation of signals are linear systems. Figure 19 shows a simple diagram of a DPSK signal.

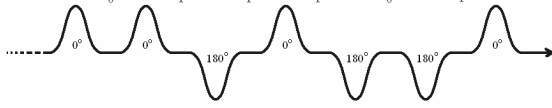


Figure 19: DPSK Pulse Train

Figure 20 gives an example of where DPSK electromagnetic wave resides in polar coordinates using phasor notation.

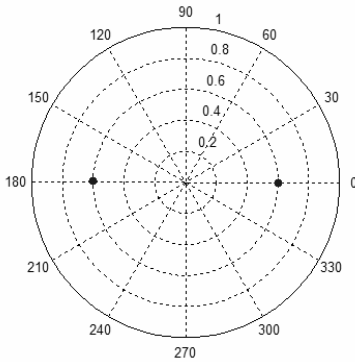


Figure 20: Data in Polar Coordinates

Since phase of an optical wave cannot be measured directly the receiver must somehow convert phase difference into some kind of measure of intensity. To do this we model a receiver shown in Figure 21 using a MZI with one arm longer than the other precisely so that at the second beam splitter the current bit of data interferes with the subsequent bit.

$$\hat{E}_{out_1} = \frac{1}{2}(\hat{E}_{n+1} - \hat{E}_n) \quad (43a)$$

$$\hat{E}_{out_2} = \frac{1}{2}j(\hat{E}_{n+1} + \hat{E}_n) \quad (43b)$$

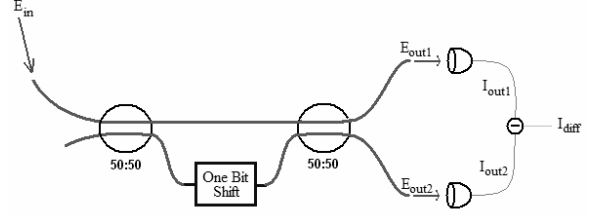


Figure 21: The DPSK Receiver

Assuming that only phase can vary by 180° between bits, E_{out_1} will have a relative amplitude of one when the two bits are out of phase and zero when they are in phase. Correspondingly, E_{out_2} will have a relative amplitude of one when the two bits are in phase and zero when they are out of phase. Using an optical power detector the magnitude of both output electric field amplitudes can be read out. By subtracting these values the receiver reads either a +1 or -1, this value is called I_{diff} .

$$I_{diff} = |\hat{E}_{out_1}|^2 - |\hat{E}_{out_2}|^2 \quad (44)$$

2.8i Noise in DPSK

Since all systems are affected by noise, it is important to understand the noise's effect on signal quality and error probability when it comes to DPSK. We will be using a very simple model to quantify the noise experienced by a traveling signal. There will be two types of noise, amplitude and phase. Both will be normally and randomly distributed with a mean of zero and a predetermined standard deviation. Larger standard deviations correspond to more noise. Phase noise will range in standard deviation from 0° - 20° and amplitude noise will range in standard deviation from 0%-30%. The equation we will be using to add noise will be:

$$\hat{E}_{after} = \hat{E}_{before} \cdot (1 + N_A) \cdot e^{jN_P} \quad (45)$$

Where N_A describes amplitude noise and N_P describes phase noise.

This model will be applied independently from bit to bit as data is traveling along a noisy line. Bits will be generated randomly and then the noise will be applied randomly. The effects of noise can be easily seen in polar coordinates, shown below.

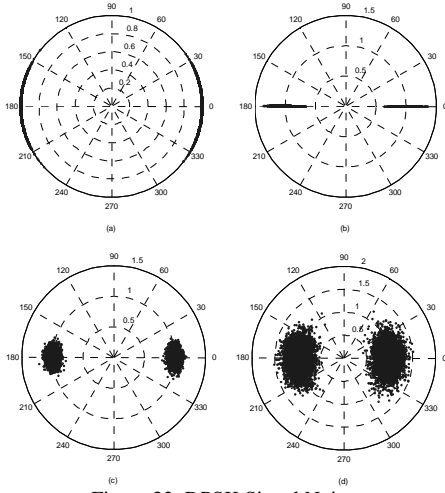


Figure 22: DPSK Signal Noise

(a) $N_P=10, N_A=0$ (b) $N_P=0, N_A=10$
(c) $N_P=5, N_A=5$ (d) $N_P=15, N_A=15$

Figure 23 shows a histogram of received data, I_{diff} , with Gaussian fits after two stages of noise both with $N_P=20$ and $N_A=20$. The curves are centered at about ± 1 and appear to be normally distributed. In all cases our curves will be approximately symmetric about zero. Therefore we can split the I_{diff} data at zero and do Gaussian fits to each curve separately to find the mean and variance of each. These values can then be used to measure the data quality.

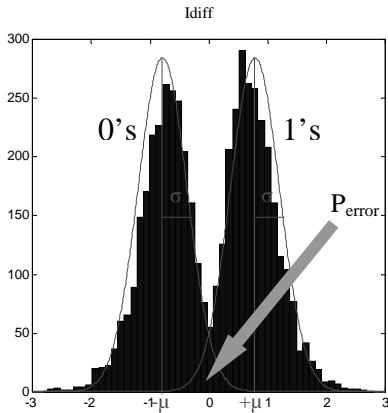


Figure 23: Received data, I_{diff} , for $N_A=20, N_P=20$

A good measure of signal to noise ratio (SNR) is the quality factor (Q-factor) of the data. The equation for the Q-factor that we will be using is expressed below.

$$Q = \frac{\mu}{2\sigma} \quad (46)$$

Where μ is mean and σ is standard deviation.

Another good measure of the quality of a signal is the expected probability of the receiver misreading the data. For our purposes an error occurs when data that belongs grouped with +1 is received with an I_{diff} less than zero and is therefore grouped with -1 or vice versa. The probability of receiving an I_{diff} less than zero is found by simply calculating the CDF of our fitted Gaussian curve with standard deviation (σ) and mean ($+\mu$). The probability of this error will be called P_{error} . In modern communication systems the allowable probability of an error is usually 10^{-9} or 10^{-6} . In the case of our data shown in Figure 23, $P_{error} = 10^{-0.7535}$. Similarly the Q-factor is 0.6794. This data is way too noisy to pass communication standards. The importance of a regenerative device for this kind of problem is evident.

2.8ii DPSK Regeneration

Regeneration is the act of cleaning up a signal along the path of propagation in order to minimize the noise seen by the receiver. A simple way of modeling data regeneration and comparing it to non-regenerated data is shown below.

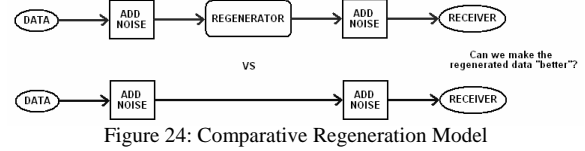


Figure 24: Comparative Regeneration Model

In our case it is important for the DPSK regenerator to clean up both phase and amplitude noise. It might also be of importance for the regenerator to amplify the signal so that attenuation experienced along the line can be remedied for future propagation.

3. Optimizing Nonlinear Media for Regeneration

3.1 Kerr Media

We will be following the steps used by Crousore et al. [5] in their publication to optimize the regenerative properties of a nonlinear MZI with Kerr media. For comparison purposes we will also be using an I_{LO} of 20mW and a γ of $27W^{-1}km^{-1}$. However, for later optimizations of different nonlinear media a thorough look into the effect of all parameters is necessary and no parameters will have a predetermined value.

The phase-sensitive amplifier already has qualities of phase regeneration. This means that phase noise at the output has been improved compared to how bad it was at the input. Driving the nonlinear device into saturation with increased signal and LO intensity causes clipping and distortion of phase-sensitive characteristics which can provide amplitude regeneration as well. This is because output amplitude is restricted in a saturated device. Saturation of a nonlinear MZI occurs as the LO pump gets depleted and no more of its power can be diverted onto the output. For other media that themselves can saturate, like the SOA and SA, nonlinear MZI saturation occurs as a combination of both effects.

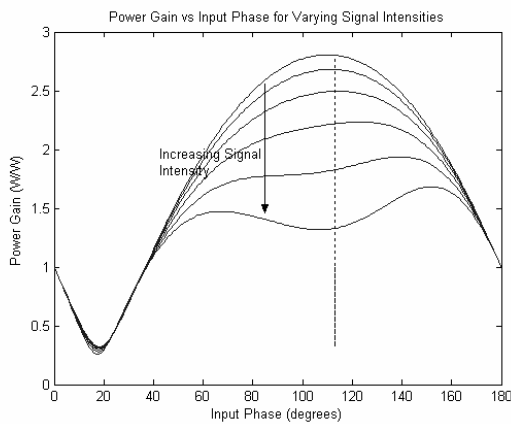


Figure 25: Effect of Increasing Signal Intensity

Figure 25 shows that as the signal intensity increases the device saturates. Gain is lost as the device saturates, however the distortion on our curves suggests that we might be able to choose an operation point where changes in input phase do not change the output power significantly. This would minimize phase-to-amplitude noise in our device. Another important observation of this graph is that even as signal intensity changes, the input phase difference of interest remains approximately the same at around 113°. If we choose the phase difference to be this value we can see the saturation effect on a single plot.

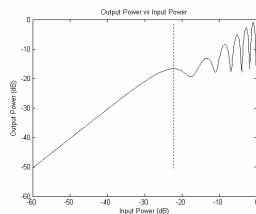


Figure 26a: Signal Intensity Going into Saturation

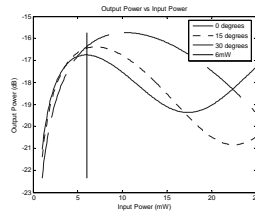


Figure 26b: Signal Intensity with different phases

From Figure 26a we see that our device begins to saturate around the dotted line which corresponds to an input of approximately 6mW. Setting our signal intensity at this value would insure low amplitude-to-amplitude noise. A close up view with the input phase varying is shown in Figure 26b. Figure 26b also shows that the phase-to-amplitude noise, shown by the different phases, is relatively small at this peak going into saturation.

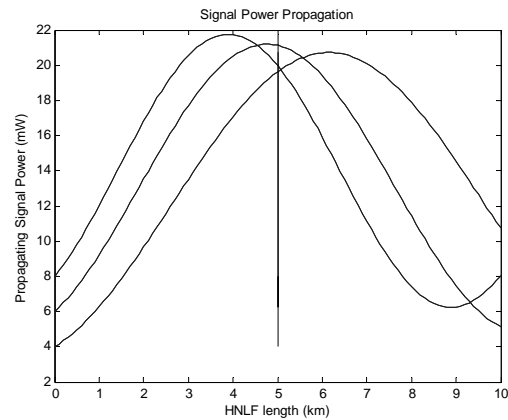


Figure 27: Signal Propagation to find Fiber Length

Figure 27 shows the propagation of three signals with initial power of 4, 6, and 8mW with 6mW being of highest interest. This signal has peak output and is closest to the 4mW and 8mW signals when the fiber is 5km long. This optimization of length not only maximizes gain but also cleans up amplitude-to-amplitude noise.

The final parameters for our operation point are:

$$\begin{aligned}
 I_{SIG} &= 6 \text{ mW} \\
 I_{LO} &= 20 \text{ mW} \\
 \text{Phase} &= 113^\circ \\
 \gamma &= 27 \text{ W}^{-1} \text{ km}^{-1} \\
 L &= 5 \text{ km}
 \end{aligned}$$

Figure 28 shows two-dimensional graphs at the operation point that describe all four types of noise improvement. The effects of changing input phase and amplitude can be seen for the output.

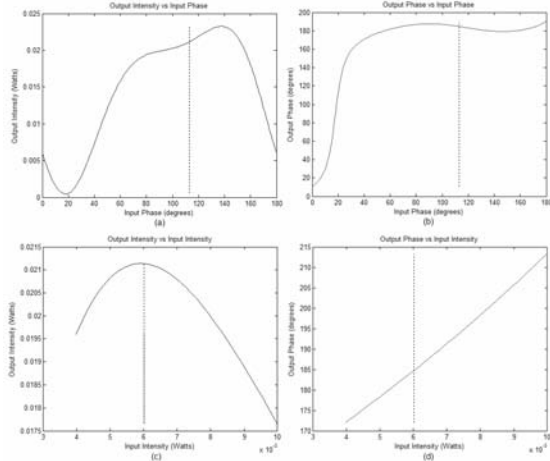


Figure 28: Noise Improvement
 (a) Phase-to-Amplitude (b) Phase-to-Phase
 (c) Amplitude-to-Amplitude (d) Amplitude-to-Phase

3.2 Saturable Amplifier Media

In order to optimize the SOA based MZI regenerator all five parameters: I_{LO} , I_{SIG} , phase, α_H , and g_0L must be adjusted. To start off lets see how increasing signal intensity into saturation affects the look of the phase-sensitive amplification figure.

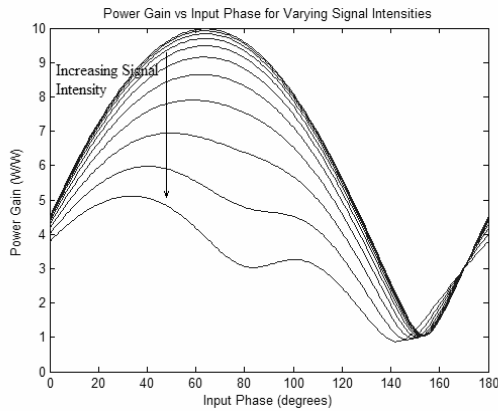


Figure 29: Effect of Increasing Signal Intensity

Figure 29 shows how the phase-sensitive amplification features of the SOA MZI are affected as the signal increases into the saturation region. Comparison with Figure 25 shows that the SOA graph is not as tight as and more lopsided than the HNL graph. Phases of interest are not readily apparent, however inflection points seem to reside around 90° .

Since our α_H and g_0L parameters have a certain range associated with them for actual SOAs, it wont be hard to manually change them along with I_{LO} to

see different three-dimensional graphs of I_{SIG} and phase as they relate to output phase and amplitude. What we want is a graph where change in phase and amplitude at the input have a small effect on the phase and amplitude at the output, thus effectively reducing both types of noise.

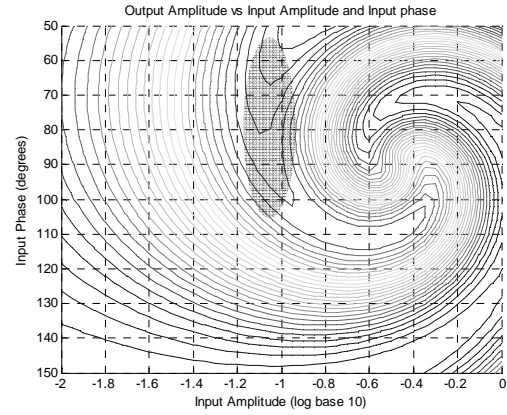


Figure 30a: Output Amplitude for Varying Input Amplitude and Phase

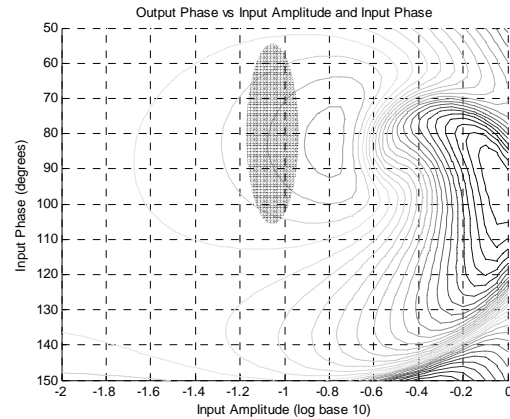


Figure 30b: Output Phase for Varying Input Amplitude and Phase

Figures 30a and 30b show contour plots of output amplitude and phase for a range of input phases and amplitudes. The shaded area corresponds to a region of interest where both output amplitude and phase vary by a small amount for a range of input amplitude and phase. In both figures the input amplitude is in terms of I_{SAT} which we designated to be $1mW$.

A good operation point for our SOA design would be:

$$\begin{aligned}
 I_{SIG} &= 80 \mu W \\
 I_{LO} &= 320 \mu W \\
 \text{Phase} &= 80^\circ
 \end{aligned}$$

$$\alpha_H = 4$$

$$g_0L = 5$$

Figure 31 shows two-dimensional graphs at the operation point that describe all four types of noise improvement. The effects of changing input phase and amplitude can be seen for the output.

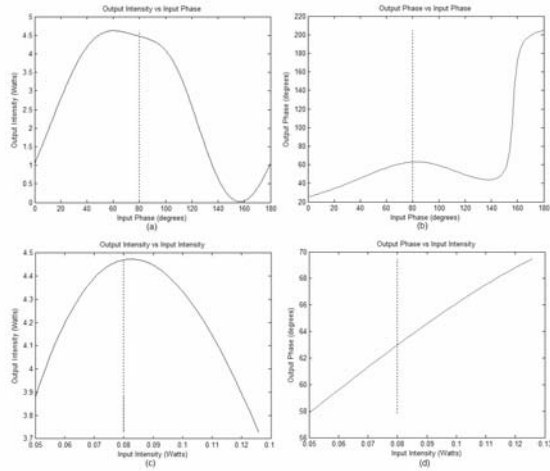


Figure 31: Noise Improvement
 (a) Phase-to-Amplitude (b) Phase-to-Phase
 (c) Amplitude-to-Amplitude (d) Amplitude-to-Phase

3.3 Saturated Absorber Media

The saturable absorber is going to be optimized just like the SOA with all five parameters tweaked to provide the best regeneration.

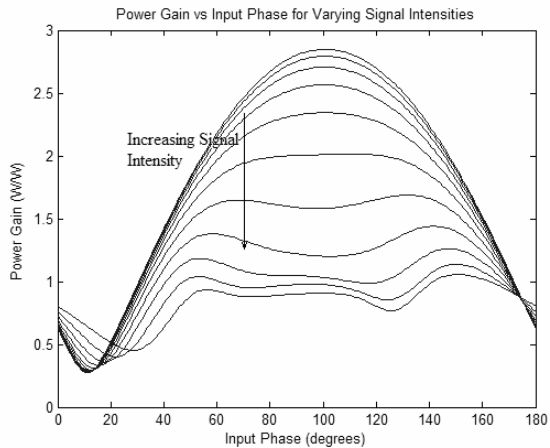


Figure 32: Effect of Increasing Signal Intensity

The graph in Figure 32 seems just as loose as Figure 29 with the SOA, however, like the HNFLF in Figure 25, Figure 32 does not seem very lopsided. In

fact, with the SA it seems like we could create a very symmetric and plateau-like phase-sensitive amplifier.

We can find three dimensional contour plots of output phase and output amplitude as functions of input phase and input amplitude and find regions where noise can be filtered out.

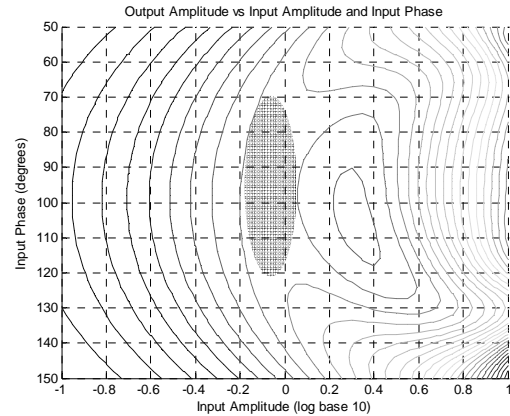


Figure 33a: Output Amplitude for Varying Input Amplitude and Phase

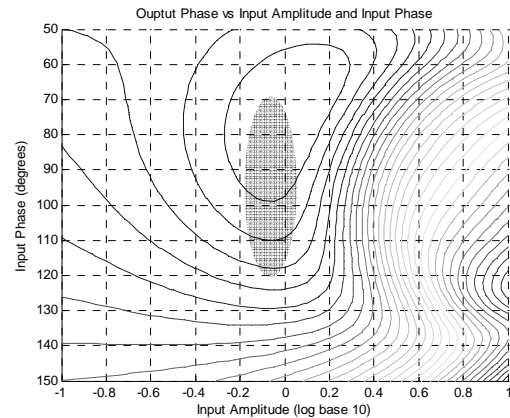


Figure 33b: Output Phase for Varying Input Amplitude and Phase

In both Figures 33a and 33b the shaded area corresponds to our region of interest and the input amplitude along the x-axes is in terms of I_{SAT} . It is worthwhile to note that the LO has an intensity ten times stronger than that of I_{SAT} and by looking at the graphs our input intensity of interest seems to be just less than I_{SAT} . This device is therefore heavily in the saturation region.

A good operation point for our SA design would be:

$$I_{SIG} = 0.9mW$$

$$I_{LO} = 10mW$$

$$Phase = 95^\circ$$

$$\alpha_0 L = 4.5$$

$$\alpha_H = 4$$

Figure 34 shows two-dimensional graphs at the operation point that describe all four types of noise improvement. The effects of changing input phase and amplitude can be seen for the output.

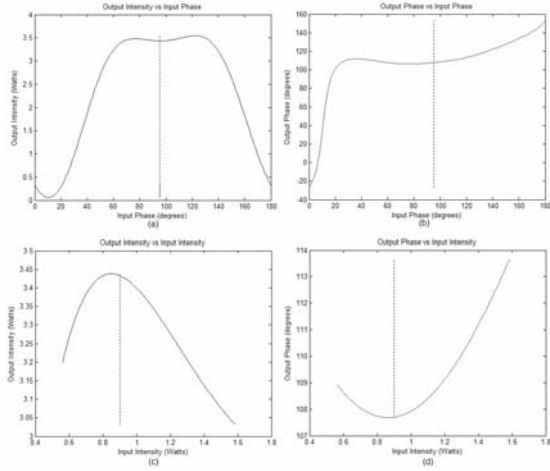


Figure 34: Noise Improvement
 (a) Phase-to-Amplitude (b) Phase-to-Phase
 (c) Amplitude-to-Amplitude (d) Amplitude-to-Phase

3.4 Two-Photon Absorber Media

As was seen in Section 2.7, the TPA-based device might not distort asymmetrically like the previous three since the TPA does not provide nonlinear phase shifts.

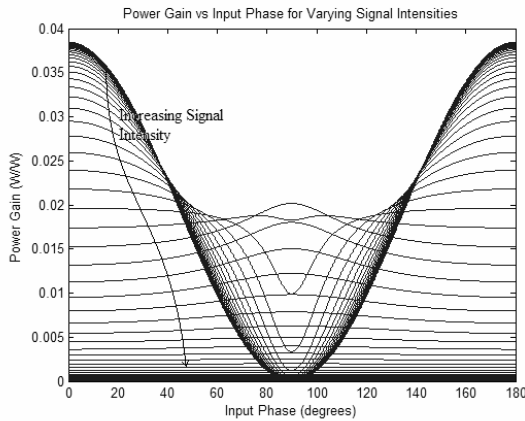


Figure 35: Effect of Increasing Signal Intensity

Figure 35 shows how the power gain is distorted with increasing signal intensity. Nothing of interest happens as input intensities saturate that would signify that the TPA-based nonlinear MZI can be opti-

mized for both phase and amplitude regeneration. Subsequently, we will analyze the TPA-based MZI in its non-saturation regime as a phase-sensitive amplifier and see how well it regenerates a DPSK signal.

The parameters that we will be using are:

$$I_{SIG} = 0.1\text{mW}$$

$$I_{LO} = 10\text{W}$$

$$\text{Phase} = 180^\circ$$

$$\alpha_2 L = 10$$

Figure 36 shows two-dimensional graphs at the operation point that describe all four types of noise improvement. The effects of changing input phase and amplitude can be seen for the output.

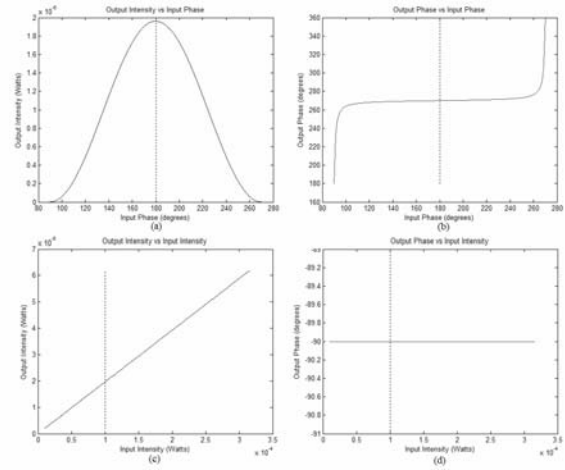


Figure 36: Noise Improvement
 (a) Phase-to-Amplitude (b) Phase-to-Phase
 (c) Amplitude-to-Amplitude (d) Amplitude-to-Phase

4. Results

4.1 Kerr Media Results

By using the optimized parameters described in Section 3.1 we simulated the regeneration of many data bits randomly placed in polar coordinates at 0° and 180° . Amplitude and phase noise was then introduced. For simulation we chose phase and amplitude noise to be 10° and 10% respectively. The data was then either regenerated or not and then further noise of the same amount was introduced.

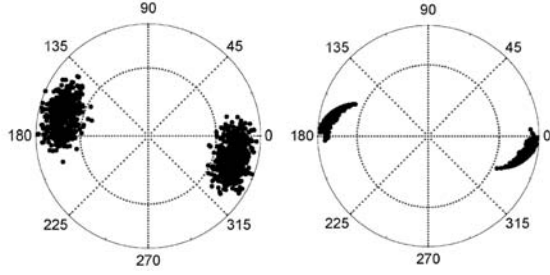


Figure 37: Published Results Before and After Regeneration

The results of Croussore et al.'s paper [5] are displayed in Figure 37. It shows data before, on the left, and immediately after regeneration, on the right. Comparative results using our model are shown dark in Figures 38 and 39 below. As expected the results look very similar.

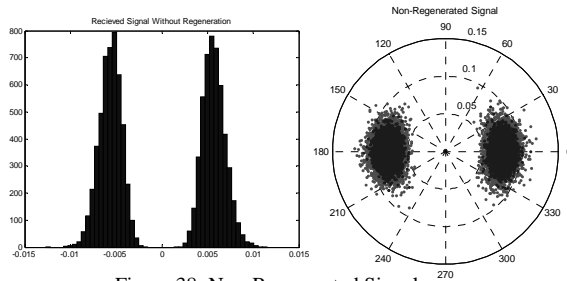


Figure 38: Non-Regenerated Signal

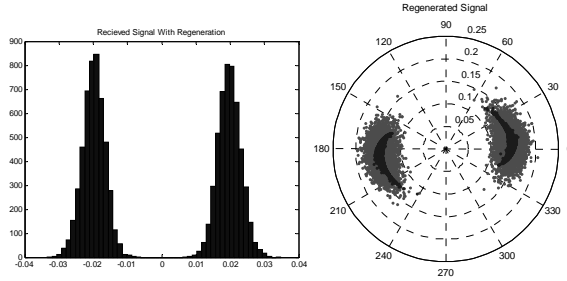


Figure 39: Regenerated Signal

The graphs in Figures 38 and 39 show histograms of the received data and polar graphs of the data along the line of propagation. In the polar graphs, the dark areas corresponds to the simulated data before the second round of adding noise and the light areas correspond to that same simulated data after the second round of noise. The effect of regeneration can be seen comparing the dark data, while the light data is essentially what the receiver sees. Comparing the graphs, obvious regeneration is achieved.

$N_S = N_P = 10$	Q	P_{error}
Non-Regenerated	2.2557	$10^{-5.1909}$
HNLF Regenerated	3.0302	$10^{-8.8674}$

Table 1: Quantification of HNLF Regeneration

Table 1 tells us that without regeneration our data would not have met the communication requirement of less than 10^{-6} probability of error, however with HNLF regeneration this is easily met.

By looking at the dark data in the polar graph of Figure 39 we can get an idea of some of the flaws in the HNLF MZI regenerator. Phase noise is still very noticeable after our regeneration. Looking back at Figure 28d it is apparent that what we are seeing in our output is a result of poor amplitude-to-phase noise reduction. All other noise improvements seem to do fairly well.

4.2 Saturable Amplifier Results

The SOA-based nonlinear MZI regenerator is simulated using the same phase and amplitude noise values that were used in the HNLF setup. We now begin modeling ASE noise for our simulations as described in Section 2.5iii. Our operation point is using the optimized parameters described in Section 3.2. We re-simulate the non-regenerated data. Therefore it is slightly different from what was seen for the HNLF model.

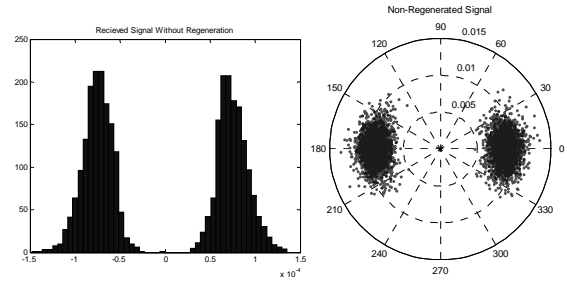


Figure 40: Non-Regenerated Signal

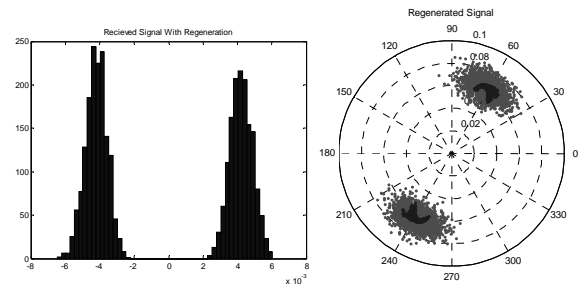


Figure 41: Regenerated Signal

The graphs in Figures 40 and 41 correspond to those in Figures 38 and 39 for the HNLF model. Immediately it looks like the SOA-based device re-

generated better than the HNLF one. Further analysis supports this.

$N_S = N_P = 10$	Q	P_{error}
Non-Regenerated	2.2425	$10^{-5.1372}$
HNLF Regenerated	3.3065	$10^{-10.4244}$

Table 2: Quantification of SOA Regeneration

In Table 2 we see that data that originally could not meet the communication requirement of less than 10^{-6} probability of error, now easily meets the requirement of a probability of error less than 10^{-9} . Therefore, our SOA-based regenerator works very well.

4.3 Saturable Absorber Results

Now, we simulate the SA-based nonlinear MZI regenerator using the optimized parameters found in Section 3.3.

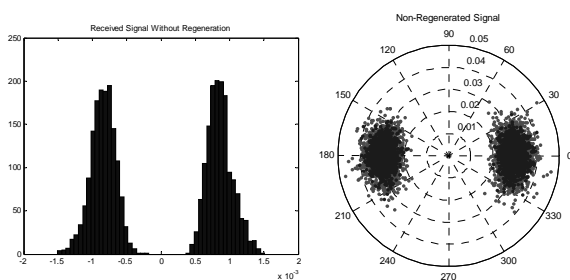


Figure 42: Non-Regenerated Signal

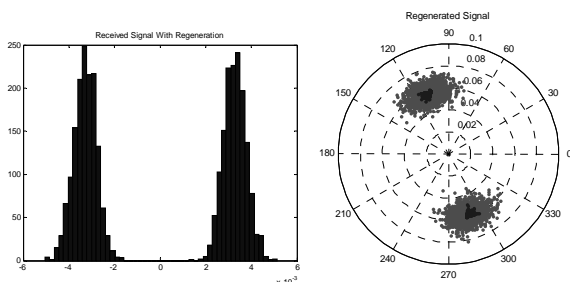


Figure 43: Regenerated Signal

The regeneration of data using a SA-based MZI, shown above, looks just as well regenerated as data that was cleaned up using the SOA-based MZI, if not more so.

$N_S = N_P = 10$	Q	P_{error}
Non-Regenerated	2.3125	$10^{-5.4263}$
HNLF Regenerated	3.3071	$10^{-10.4274}$

Table 3: Quantification of SA Regeneration

Again we see our data that originally could not meet the 10^{-6} error probability requirement, easily meets the 10^{-9} requirement with SA-based MZI regeneration.

4.4 Two-Photon Absorber Results

Using the parameters described in Section 3.4 we simulate regeneration using the TPA-based MZI. Since we are using the TPA MZI as a phase-sensitive amplifier and not in saturation, we do not expect to see as great of regeneration as was observed with the other three models.

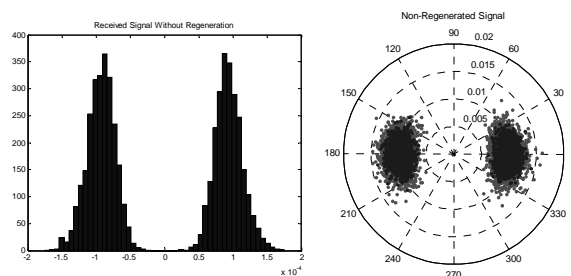


Figure 44: Non-Regenerated Signal

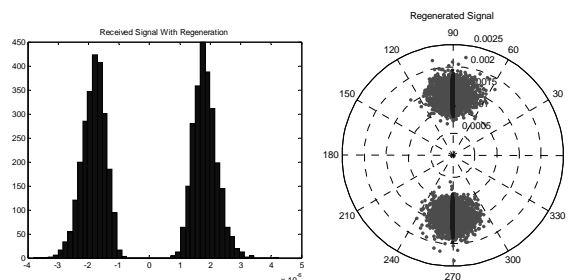


Figure 45: Regenerated Signal

Figure 45 shows that the TPA nonlinear MZI as a phase-sensitive amplifier acts to suppress phase noise at the output extremely well. However output amplitude noise is barely suppressed indicating poor DPSK regeneration. Therefore the unsaturated phase-sensitive amplifier only works well for phase regeneration.

$N_S = N_P = 10$	Q	P_{error}
Non-Regenerated	2.2763	$10^{-5.1757}$
HNLF Regenerated	2.3833	$10^{-5.7232}$

Table 4: Quantification of TPA Regeneration

Table 3 shows that DPSK regeneration using a TPA nonlinear MZI barely improves the signal.

4.5 Comparison of Nonlinear Media

Figure 46 below summarizes the regeneration experienced through all four different types of nonlinear MZIs. Each of the data points are normalized so that the overall power gain of the devices can be seen along the radial axes.

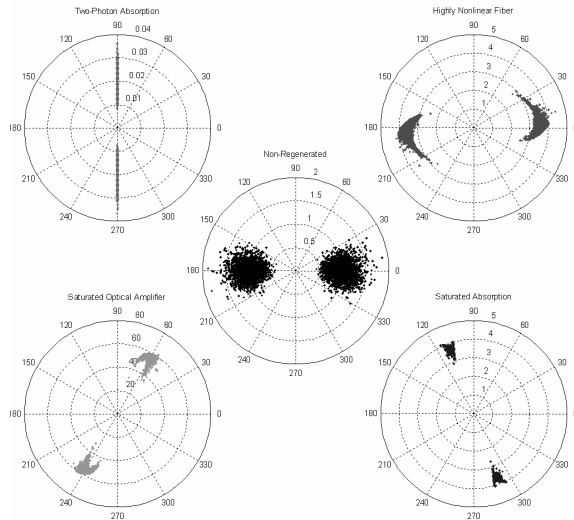


Figure 46: Comparison of Normalized Regeneration

All four models were run with varying degrees of both phase and amplitude noise and their characteristics were tabulated. Below are contour plots showing how much more noise our signals can tolerate using regeneration while still meeting certain Q -factor and P_{error} communication thresholds. There is no significance of a Q -factor = 2, it is simply used for comparison.

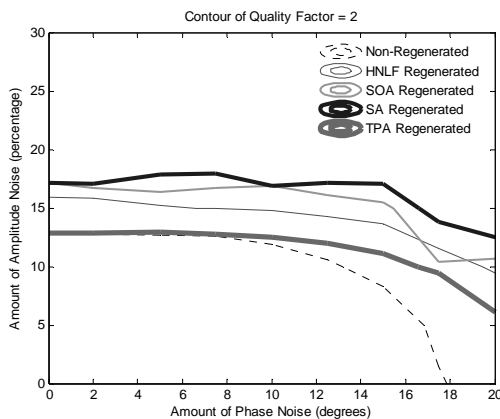


Figure 47: Q-factor Comparison

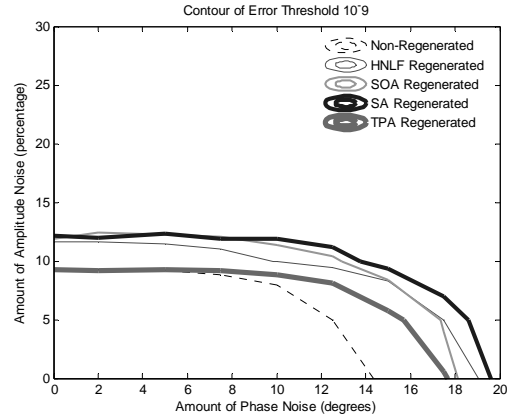


Figure 48: P_{error} Comparison

5. Discussion

Of the four different nonlinear media analyzed for the purpose of DPSK phase and amplitude regeneration, three provide significant regeneration, which includes Kerr, SOA, and SA media. The SOA and SA media provide approximately the same amount of regeneration, with the SA being slightly better. While the Kerr media provides good regeneration it does not regenerate as well as the other two. If one were to be using HNLf for regeneration purposes, they would have to consider the space requirements of using the meters to kilometers of fiber necessary for the job. Both the Kerr media and the saturable absorber provide modest signal amplification on the order of 3-4 W/W, however the SOA material provides gain in the range of 40-60 W/W. Despite this seeming advantage it might be more efficient to regenerate using the SA-based MZI and then amplify the output using only one amplifier, rather than powering the two required for the SOA-based MZI.

In their paper, Croussore et al. [5] explored the process of phase-only regeneration, using their HNLf device with intensities much less than saturation. Their results were very similar to the ones we found with our TPA. They proposed that this type of device might be well suited for pre-processing before the receiver. All four of our nonlinear media, including TPA, were able to provide phase-only regeneration and as a result could be used for this purpose.

6. Conclusion

All four of the nonlinear media analyzed in this paper provided phase-sensitive transmission, when used in a Mach-Zehnder interferometer. A simple phase-sensitive amplifier can be used to clean up phase noise, however by driving these devices into saturation both phase and amplitude noise can be reduced. Phase and amplitude noise reduction is necessary for cleaning up differential phase-shift keyed signals, which as a modulation scheme, prove to be more robust than classical on/off keying approaches. Of the four nonlinear media analyzed for this type of regeneration, three provided significant results, while one, the saturable absorber, seemed to be the most promising. Given these positive results, further research should be done to characterize these devices for physical implementation and experimentation. This includes using time-dependant models and designing a means for LO recovery from the signal.

BIBLIOGRAPHY

- [1] V.S. Grigoryan, M. Shin, P. Devgan and P. Kumar, "Mechanism of SOA-based regenerative amplification of phase-noise degraded DPSK signals" *Electronic Letters*, September 1, 2005, Vol. 41, No. 18
- [2] K. Croussore, I. Kim, Y. Han, C. Kim, G. Li, "Demonstration of phase-regeneration of DPSK signals based on phase-sensitive amplification" *Optics Express*, May 30, 2005, Vol. 13, No. 11
- [3] K. Croussore, I. Kim, Y. Han, C. Kim, G. Li, "Phase-and-amplitude regeneration of differential phase-shift keyed signals using a phase-sensitive amplifier" *Optics Express*, March 20, 2006, Vol. 14, No. 6
- [4] M. Shin, P. S. Devgan, V. S. Grigoryan, and P. Kumar, "SNR Improvement of DPSK Signals in a Semiconductor Optical Regenerative Amplifier" *IEEE Photonics Tech. Letters*, January 1, 2006, Vol. 18, No. 1
- [5] K. Croussore, C. Kim, and G. Li, "All-optical regeneration of differential phase-shift keying signals based on phase-sensitive amplification" *Optics Letters*, October 15, 2004, Vol. 29, No. 20
- [6] Siegman, A. E., 1986, *Lasers*, Mill Valley, University Science Books, Chapter 10.2
- [7] Siegman, A. E., 1986, *Lasers*, Mill Valley, University Science Books, Chapter 7.7
- [8] Semiconductor Optical Amplifiers in a non-linear Mach-Zehnder Interferometer
- [9] Siegman, A. E., 1986, *Lasers*, Mill Valley, University Science Books, Chapter 11.6
- [10] Siegman, A. E., 1986, *Lasers*, Mill Valley, University Science Books, Chapter 13.8
- [11] Siegman, A. E., 1986, *Lasers*, Mill Valley, University Science Books, Chapter 28.1
- [12] Prasad, P. N., Williams, D. J, 1991, *Introduction to Nonlinear Optical Effects in Molecules and Polymers*, New York, John Wiley & Sons, Inc. Chapter 8.1.3
- [13] W. Imajuku, A. Takada, "Gain Characteristics of Coherent Optical Amplifiers Using a Mach-Zehnder Interferometer with Kerr Media" *IEEE Journal of Quantum Electronics*, November 11, 1999, Vol. 35, No. 11